Lasers in Manufacturing Conference 2021

Remote laser welding system with automatic 3D teaching, in-line 3D seam tracking, and adaptive power control

Matija Jezeršek[a,*], Matjaž Kos[a], Erih Arko[b], Hubert Kosler[b]

[a]*University of Ljubljana, Faculty of Mechanical Engineering, Laboratory for Laser Techniques, Aškerčeva cesta 6, Ljubljana 1000, Slovenia*
[b]*Yaskawa Slovenija d.o.o., Lepovče 23, Ribnica 1310, Slovenia*

Abstract

An adaptive remote laser welding system based on triangulation feed-back control is presented. It enables off-line measuring of a workpiece 3D shape, in-line 3D seam tracking, and in-line laser power control, which are extremely important features for producing sound welds on complex geometries. The 3D measuring is done by a triangulation camera and the laser's pilot beam. The same camera is utilized to determine the 3D seam position and to monitor the key process features, including the weld depth.

Results show high 3D measuring precision in the lateral (0.05 mm) and vertical (0.3 mm) direction. Additionally, laser power control significantly reduces penetration depth and plasma oscillations. Thus, the adaptive laser welding can be used for small series and customized production of parts where a highly flexible, precise, and cost-effective joining technology is required.

Keywords: Remote laser welding; triangulation; 3D object measurement; 3D seam tracking; laser power control

1. Introduction

Remote laser welding systems (RLWS) are based on the integration of an industrial robot for rough positioning, scanning optics for precise laser beam movement and a high-intensity fiber laser. These systems enable extremely high-speed and precise welding of complex geometries over a large working area while significantly reducing non-productive positioning times. Due to these features, they allow welding of

* Corresponding author. Tel.: +386-1-4771171 .
E-mail address: matija.jezersek@fs.uni-lj.si

thin-walled lightweight structures and advanced materials, making them one of the key enabling technologies in emerging areas such as e-mobility, green technologies and electronics.

Main setbacks represent the initial system cost and time-consuming teaching of the laser beam trajectory and power regulation during simultaneous robot and beam movement. Mass customization and the use of different material combinations present a great challenge for these systems (Um and Stroud 2017; Bednar and Modrak 2014). The use of simulation tools, such as virtual robot programming environments (Hatwig et al. 2010) and numerical process simulations (Franciosa et al. 2019; Wang et al. 2011) can improve the welding quality and speed-up the teaching times. However, due to deviations between simulations and real-world situations (manufacturing and positioning tolerances) and thermal deformations during welding (Gorkič et al. 2006), manual corrections are necessary and time-consuming. These can lead to unacceptable weld quality and can lack the necessary process traceability for quality control.

Therefore, a system with the possibility of adaptive laser beam guiding along the 3D weld path and in-line power control is advantageous. Beam guiding methods are usually based on visual sensors (Malamas et al. 2003) and allow acceptable precision to determine different weld features (Poss and Ransom 2014). Among these, laser triangulation methods provide a robust and precise measurement in 3D (Muhammad et al. 2016; Regaard et al. 2009). Usually, these sensors are attached in front of the welding head which limits the working area and presents a delay in welding as the seam position is detected a few centimetres before the weld.

Furthermore, monitoring of laser interaction zone is also proving to be essential, as it helps to understand the welding process and identifies stable welding states with uniform weld parameters such as width and depth (You et al. 2013). Most common methods of monitoring are also based on visual sensors, which provide detailed 2D or 3D information of the welding process such as weld pool dynamics (Schaefer et al. 2017; Eriksson et al. 2013; Chianese et al. 2020). One of the most important weld quality estimators is penetration depth which can be measured in real-time with the principle of optical coherence tomography (OCT) (Dupriez and Denkl 2017; Sokolov, Franciosa, Al Botros, et al. 2020; Sokolov, Franciosa, Sun, et al. 2020). However, due to it being a relatively new technology, it is necessary to investigate many aspects, such as the position of the laser beam probe with respect to the welding beam, the influence of keyhole stability on the measurement and also the processing of the measured signal.

In this paper we demonstrate a concept of adaptive RLWS based on an optical triangulation feed-back control which was developed to overcome the limitation of imprecise teaching and finding the right welding parameters. The measuring principle is based on off-axis camera which acquires images of workpiece before or during laser welding where the workpiece is additionally illuminated with structured laser light. We have demonstrated in recent studies, that such a system enables off-line automatic 3D teaching of complex welding trajectories (Jezeršek et al. 2017), in-line 3D tracking of the seam position (Kos et al. 2019), and in-line laser power control during welding to produce a uniform weld-depth (Božič et al. 2020; Kos et al. 2020). In this paper we present that all three functionalities can be performed simultaneously with the same system.

2. Hardware set-up and algorithms

The RLW system with a triangulation feed-back control is shown in Fig. 1. The high-power laser light is guided through the optical fiber from the laser source (IPG, model YLR-400-AC, 400 W, continuous-wave, wavelength 1070 nm,) to the 3D scanning head (HighYAG, model RLSK, working volume of 200 mm x 300 mm x 200 mm in X, Y and Z directions, respectively), which is held by the 6-axis robot (Yaskawa, model MC2000). The scanning head camera port was utilized to coaxially connect an illumination laser (Fotona XD-2, 810 nm ± 10 nm) to the fiber laser beam path.

The scanning head can move the fiber laser's red pointer and working beam along X, Y and Z axis of the scanning head. An off-axis camera (PointGrey, model FL3-U3-13Y3M-C, 1280×1024 pix, 150 fps, sensor size ½˝,

imaging lens of 35 mm) is utilized to detect the position of the red laser pointer or the interaction zone between the working beam and workpiece depending on the process used. For 3D teaching the scanning head generates a laser stripe using the laser's red pointer while for in-line 3D tracking the coaxial illumination laser is used to further improve the visibility of surrounding surface and seam position during welding. A circular illumination area with a diameter of 18 mm was achieved. Thus, there a two distinct processes:

- a) if the systems works in 3D teaching mode, then a band-pass filter of central wavelength of 660 nm (FWHM = 10 nm) is used for detection of the red laser stripe generated by the laser pointer (Jezeršek et al. 2017).
- b) if the system works in in-line 3D tracking and power control mode, then a band-pass filter of central wavelength of 810 nm (FWHM = 10 nm) is used to monitor the illuminated interaction zone between the welding laser beam and workpiece (Kos et al. 2019, 2020).

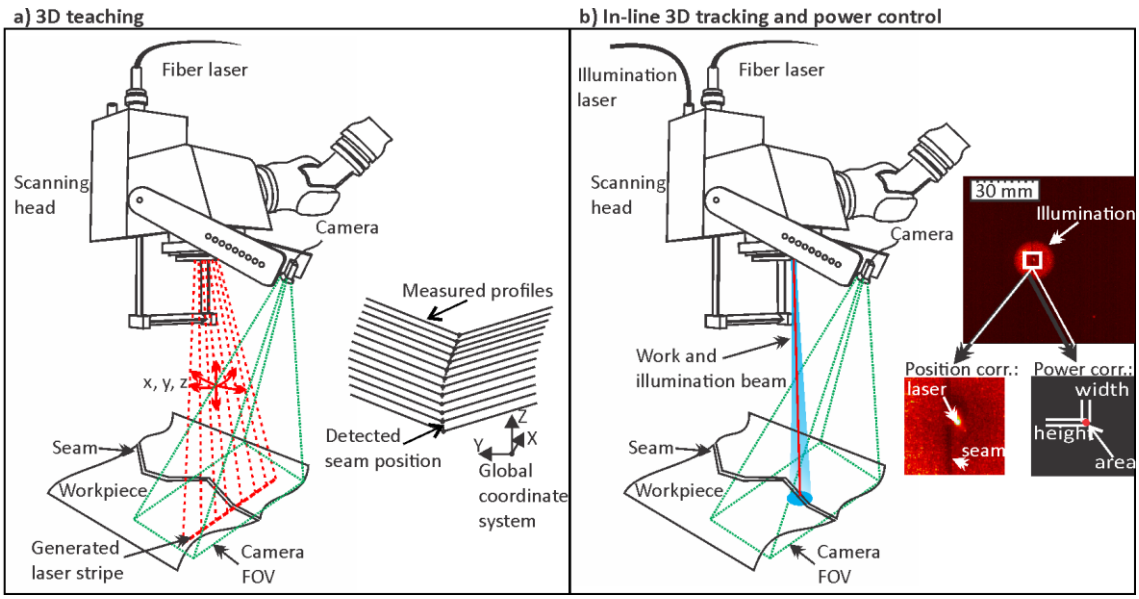

Fig. 1. Schematic presentation of the system for 3D teaching mode using generated red laser stripe and camera with 650 nm filter (a) and in-line 3D tracking and power control mode with additional illumination laser and same camera with 810 nm filter (b).

2.1. Off-line 3D teaching of welding trajectory

Precise detection of laser welding trajectory is particularly important in case of butt or fillet weld geometry, where misalignment in laser beam position can lead into low strength or failed welds. The 3D teaching process begins by visually determining the starting and ending points of the trajectory. These two points serve to limit the weld along the seam line, while the position in the transverse direction is precisely determined automatically based on the measured profiles as for all intermediate measured profiles.

The procedure for 3D trajectory determination consists of two steps: (i) contour extraction from measured 3D profiles stored in X, Y, Z, and intensity matrices, and (ii) trajectory post-processing for noise minimization and processing speed equalization. The algorithm is shown in Fig. 2(a) and described in more details in (Jezeršek et al. 2017).

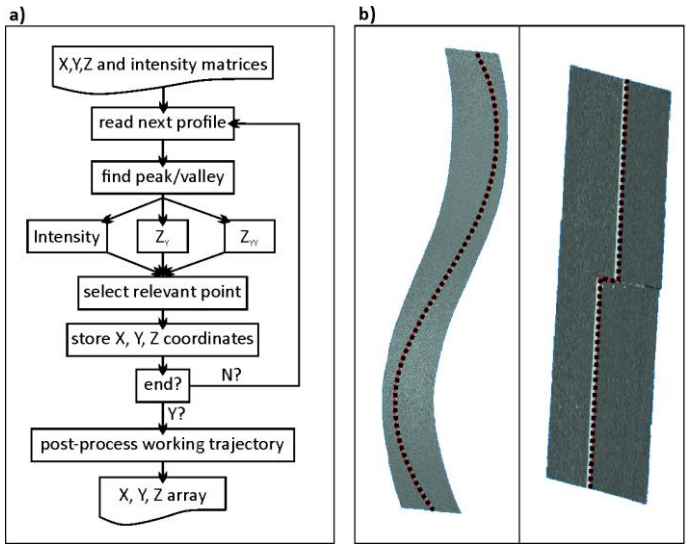

Fig. 2. Algorithm for 3D welding trajectory detection (a) and examples of 3D measurements of workpieces with detected welding trajectory (b).

Every profile, which is stored in matrices as a single row, is read and seam location is found based on peak/valley detection along the profile where the intensity, depth, and second derivative of the depth signal are used. In case of multiple peak detection, the point representing the seam location is determined as the nearest one to the point in the previous profile. The array of detected seam positions is filtered using a median filter at the end to remove possible outliers which originate from random laser light reflections. Fig. 2(b) shows examples of raw 3D measurement of workpiece and detected welding trajectories.

The 3D transformation of measured profiles into a robot's coordinate system is made using the same formulation as presented in (Pavlovčič et al. 2021). The system calibration (camera position and orientation relative to the scanning head, lens distortion, focal length, and scanning head pose relative to the robot head) is based on multiple measurements of a reference groove-shaped geometry and numerical optimization of deviation between measured and reference geometry by variation of transformation parameters.

2.2. In-line 3D seam tracking and power control

The next level of laser welding control is in-line laser beam positioning and power control according to the disturbances such as system inaccuracies, thermal deformations of workpiece and material variations in terms of light absorption and thermal properties. The necessary steps for correcting the laser beam position according to the seam 3D position and power control are shown in Fig. 3. The algorithm consist of: (i) detecting the keyhole and its shape and size on the acquired image, (ii) extrapolating the detected seam curve to the nearest point relative to the keyhole and (iii) and calculating the new laser position and power.

The detection of the keyhole starts with a robust recognition of the illumination laser beam on the workpiece, as it is coaxial with the welding beam and substantially larger in diameter. The exact keyhole location is determined within illuminated area based on adaptive threshold filtering (95% of the maximum detected intensity within illumination area). But because of spatters and plasma (these also cause overexposure) a Gaussian filter is applied prior to threshold. The keyhole location (u_k, v_k) is then calculated as the centroid of the remaining pixels.

The next step is seam detection, which is searched within the area of size O_x x O_y, positioned just below the keyhole. The possible locations of the seam are detected in all rows of the search area, where a peak/valley detection algorithm is used according to the change in intensity. These seam locations are then used for seam curve approximation using a least square algorithm. The approximated seam curve is finally used to calculate the closest location of the seam edge to the keyhole. We also consider an offset of *dv* (look ahead distance) from the detected keyhole location to reduce system response time. The closest location is then transformed to 3D coordinate system of the scanning optics and sent to the robot controller, where the same 3D transformation model is used as in case of off-line 3D teaching mode.

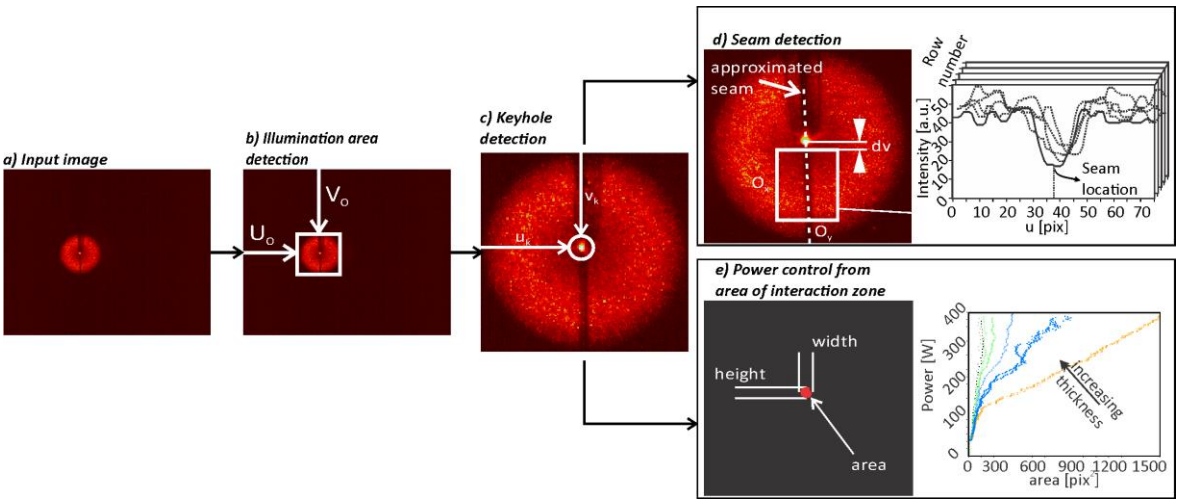

Fig. 3. Algorithm of simultaneous 3D seam tracking and laser power control algorithm. First, the larger illumination area is detected with averaging according to rows and columns (b). From detected keyhole (c), the seam position (d) and keyhole shape (e) is detected from which the new laser focus position and power is calculated.

Finally, the laser power is regulated according to the estimated penetration depth where the area of interaction zone (which includes keyhole and melt pool) is used as an estimator. For that reason, the image after threshold operation is processed with two repeated morphological operation of opening (erosion and dilation). After that the area is measured as a number of nonzero pixels.

Macrographic analyses of measured weld depth showed linear relation between the weld depth and area of interaction until full penetration is achieved. Therefore, the relation between penetration depth and the area of interaction was calibrated for various welding speeds (from 25 cm/min to 150 cm/min) and steel plate thicknesses (from 0.6 mm to 2 mm) by linearly varying the laser power from minimal to maximal power and back to minimal during each weld. Polynomial two dimensional approximation was then used to relate above parameters (Kos et al. 2020).

3. Results and discussion

To demonstrate the precision of 3D teaching mode a characteristic specimen with an overlap seam geometry was measured 21 times. The left-hand side of Fig. 4 shows the measured 3D surface of a wavy sinusoidal shape, with the detected seam trajectory coloured in red. A scanning speed of 50 cm/min was used. The rolled steel plate has dimensions of 460 × 200 × 2 mm. The scanning frequency was 40 profiles/s and the scanning width was 100 mm in all experiments. The centre of Fig. 4 shows the magnified results of the scanned

wavy specimen in an interval between 50 and 80 mm after the start of scanning and the right-hand side shows the standard deviation transversal to the scanning direction in the same interval. The top graphs show the XY projection of the detected trajectories and the bottom graphs show the XZ projection. The average standard deviations transversal to the scanning direction for the whole scan along the Y ($\overline{\sigma_Y}$) and Z ($\overline{\sigma_Z}$) axes versus are 26 µm and 181 µm respectively. This indicates sufficient measuring precision for teaching the laser welding trajectory.

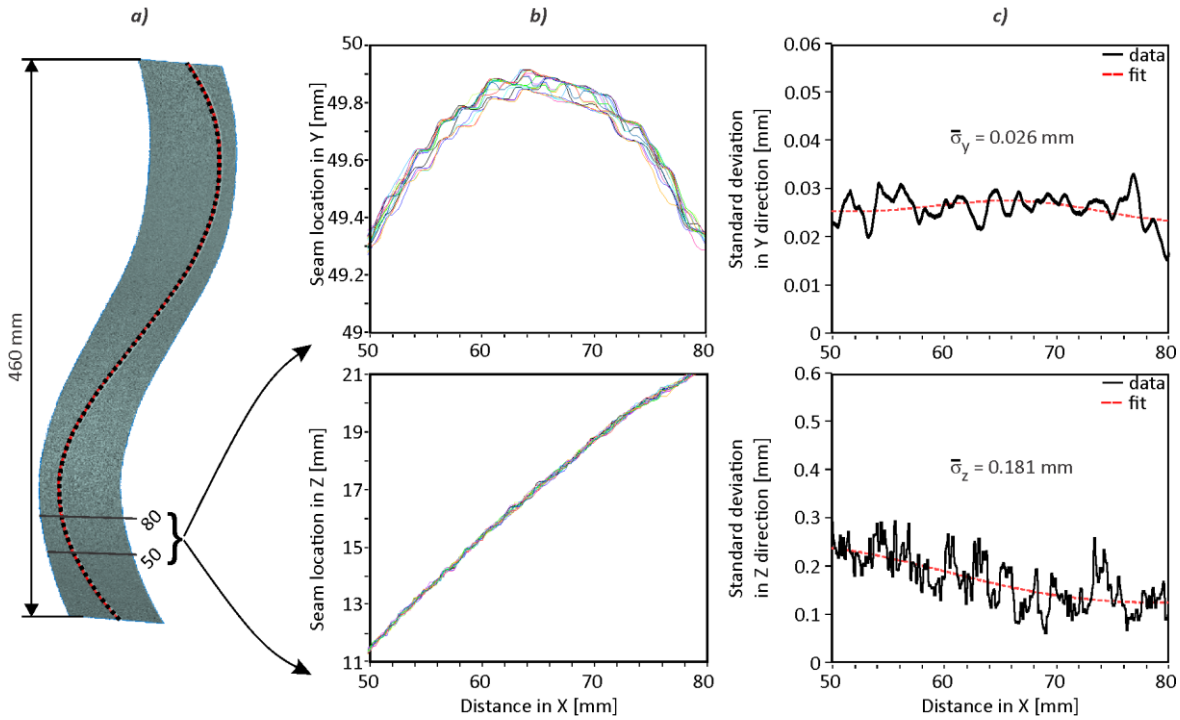

Fig. 4. Example of a wavy sine 3D measurement specimen in lap configuration (a). The red line shows the detected working trajectory. Repeatability (N=21) of sinusoidal trajectory detection (b). Averaged standard deviation of trajectories transversal to the scanning direction from all measurements (c). Data between distance 50 and 80 mm is shown for better resolution.

Fig. 5 shows the result of 3D measurement and in-line 3D seam tracking of an edge seam welding. Schematic situation and positioning of the workpiece is shown on Fig. 5(a). The 3D measured surface around the edge seam is shown on Fig. 5(b). From this measurement, the seam trajectory, located in the middle of the two plates is detected (yellow dashed curve). This information is further utilized to determine the initial position of the workpiece in the working area of the laser welding system. Fig. 5(c) shows difference between the actual laser beam position during welding (red curve) and the off-line measured (black curve). The difference appears due to thermal deformations of the workpiece during laser welding, which are efficiently compensated with the in-line 3D seam tracking. Maximal deformation was measured at the end point and was greater than 1 mm. Without the in-line seam tracking the laser beam would completely miss the target seam. The welding result is shown in Fig. 5(d) and deviation between actual weld center and seam location in Fig. 5(e). An average deviation was less than 0.03 mm with a standard deviation of less than 0.05 mm. As seen from magnified photo on Fig. 5(d) the weld was correctly made which demonstrates precise functioning of the system.

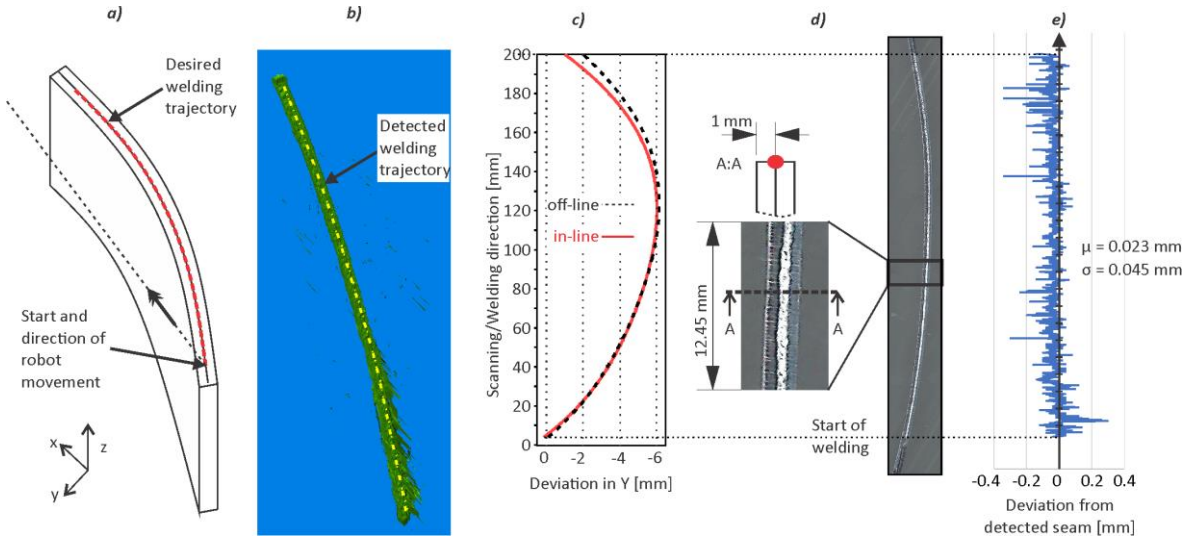

Fig. 5. Schematic presentation of welding situation of flat edge seam (a). 3D measurement and detected welding trajectory (b). Comparison between off-line (black) and in-line (red) measured trajectories (c). Welding results of the scanned flat edge seam (d). The deviation between the weld center and in-line measured trajectory along entire weld (e).

The cluster graph in Fig. 6(a) shows the relation between the laser power and measured area for desired penetration depth and welding speed. Dashed lines going from top to bottom present the approximated estimator/power values for fixed penetration depths, while dotted lines going from bottom left to top right show the change in values for different welding speeds. The lines are approximated according to the data collected from the calibration procedure. The trend of the estimator was determined for material thicknesses of less than 1.5 mm. For greater penetration depths this could not be determined due to system limitations (maximum laser power of 400 W).

Welding without and with the power-control was conducted on a 1.6 mm thick lap joint at 60 cm/min in order to compare results and determine the adequacy of the power calibration. Fig. 6(b) shows a section of the macrographic results for welding without power control, while Fig. 6(c) shows results for welding with the developed power-control algorithm. The desired weld depth was 1.2 mm (75 % of material thickness). Welding at 231 W should be carried out in order to achieve this penetration (as determined from previous experiments).

The graphs above the macrographies display the overall progress of the detected estimator for the whole welding. For power control, power progress of algorithm is also displayed. The white region corresponds to the presented macrographies. In both cases, an interaction area of approximately 100 a.u. was achieved. The power-control algorithm achieved laser power of about 231 W with slight decrease in power when the estimator value enlarges. These enlargements coincide with laser-induced plume bursts, which did not occurred if power control was used. In case of constant power, these burst result in sections with less penetration, as can be observed in Fig. 6(b). With power control a penetration depth of maximum 1.15 mm was achieved which is less than 5% relative deviation to the desired value.

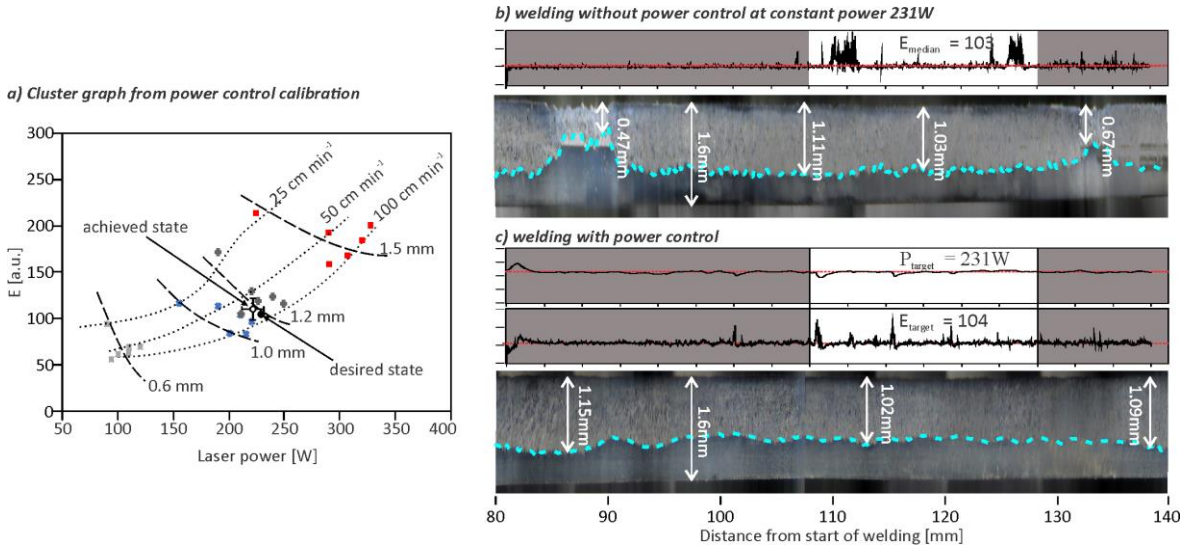

Fig. 6. Cluster graph depicting laser power needed for full penetration at different welding parameters – material thickness, and welding speed (a). Result of welding without power control (b) and comparison to the welding with the power control (c) on a 1.6 mm lap weld at 60 cm/min with a set weld depth of 1.2 mm. Graphs show the monitored interaction area during welding (both cases) and sent laser power (power control). Macrographies present a section of the made weld where they correspond with white regions shown on above graphs. Blue dashed curves mark the penetration depth.

4. Conclusions

An innovative remote laser welding system for automatic 3D teaching, in-line 3D seam tracking, and laser power control was developed based on an optical triangulation feed-back loop where off-axis camera and coaxial illumination was used. The same camera is utilized to monitor the interaction zone itself, to analyze key process features to determine and control the weld depth in real-time.

Results show that the system can automatically detect seam with precision 0.05 mm in the lateral and 0.3 mm in vertical direction which is sufficient for remote laser welding applications. Additionally, laser power control significantly reduces penetration depth (accuracy better than 5%) and plasma oscillations. Comparing to the present state of the art, developed system can significantly reduce teaching time, thus, it can be effectively used for small series and customized production of parts where a highly flexible, precise, and cost-effective joining technology is required. With further software development the system could be used also for post-process quality control, as it enables precise measurement of the 3D product shape.

Acknowledgements

The presented research work is financially supported from the GOSTOP program, contract number C3330-16-529000, co-financed from Slovenia and EU under ERDF and from the Slovenian Research Agency (research core funding No. P2-0392). We would like to thank also Yaskawa Slovenia for supplying their commercially available robotic system for remote laser-welding applications.

References

Bednar, S., & Modrak, V. (2014). Mass customization and its impact on Assembly process´ complexity. *International Journal for Quality Research*, *8*(3), 417–430.

Božič, A., Kos, M., & Jezeršek, M. (2020). Power control during remote laser welding using a convolutional neural network. *Sensors (Switzerland)*, *20*(22), 1–15. https://doi.org/10.3390/s20226658

Chianese, G., Franciosa, P., Nolte, J., Ceglarek, D., Patalano, S. (2020). Photodiode-based in-process Monitoring of Part-to-part gap and weld Penetration Depth in remote laser welding of Copper-to-steel Battery Tab Connectors. *Proceedings of the ASME 2021, 16th International Manufacturing Science and Engineering Conference (MSEC'2021)*.

Dupriez, N. D., & Denkl, A. (2017). Advances of OCT Technology for Laser Beam Processing. *Laser Technik Journal*, *14*(4), 34–38. https://doi.org/10.1002/latj.201700021

Eriksson, I., Powell, J., & Kaplan, A. F. H. (2013). Melt behavior on the keyhole front during high speed laser welding. *Optics and Lasers in Engineering*, *51*(6), 735–740. https://doi.org/10.1016/j.optlaseng.2013.01.008

Franciosa, P., Palit, A., Gerbino, S., & Ceglarek, D. (2019). A novel hybrid shell element formulation (QUAD+ and TRIA+): A benchmarking and comparative study. *Finite Elements in Analysis and Design*, *166*, 103319. https://doi.org/10.1016/j.finel.2019.103319

Gorkič, A., Jezeršek, M., Možina, J., & Diaci, J. (2006). Measurement of weldpiece distortion during pulsed laser welding using rapid laser profilometry. *Science and Technology of Welding and Joining*, *11*(1), 48–56. https://doi.org/10.1179/174329306X77065

Hatwig, J., Reinhart, G., & Zaeh, M. F. (2010). Automated task planning for industrial robots and laser scanners for remote laser beam welding and cutting. *Production Engineering*, *4*(4), 327–332. https://doi.org/10.1007/s11740-010-0252-3

Jezeršek, M., Kos, M., Kosler, H., & Možina, J. (2017). Automatic teaching of a robotic remote laser 3D processing system based on an integrated laser-triangulation profilometry. *Tehnički vjesnik*, *24*(1), 89–95. https://doi.org/10.17559/TV-20160504230058

Kos, M., Arko, E., Kosler, H., & Jezeršek, M. (2019). Remote laser welding with in-line adaptive 3D seam tracking. *The International Journal of Advanced Manufacturing Technology*. https://doi.org/10.1007/s00170-019-03875-z

Kos, M., Arko, E., Kosler, H., & Jezeršek, M. (2020). Penetration-depth control in a remote laser-welding system based on an optical triangulation loop. *Optics and Lasers in Engineering*, 106464. https://doi.org/10.1016/j.optlaseng.2020.106464

Malamas, E. N., Petrakis, E. G. M., Zervakis, M., Petit, L., & Legat, J.-D. (2003). A survey on industrial vision systems, applications and tools. *Image and Vision Computing*, *21*(2), 171–188. https://doi.org/10.1016/S0262-8856(02)00152-X

Muhammad, J., Altun, H., & Abo-Serie, E. (2016). Welding seam profiling techniques based on active vision sensing for intelligent robotic welding. *The International Journal of Advanced Manufacturing Technology*, *88*(1–4), 127–145. https://doi.org/10.1007/s00170-016-8707-0

Pavlovčič, U., Arko, P., & Jezeršek, M. (2021). Simultaneous Hand–Eye and Intrinsic Calibration of a Laser Profilometer Mounted on a Robot Arm. *Sensors*, *21*(4), 1037. https://doi.org/10.3390/s21041037

Poss, M. G., & Ransom, L. T. (2014, June 26). Remote laser welding. http://www.google.com/patents/US20140175068. Accessed 11 March 2016

Regaard, B., Kaierle, S., & Poprawe, R. (2009). Seam-tracking for high precision laser welding applications—Methods, restrictions and enhanced concepts. *Journal of Laser Applications*, *21*(4), 183. https://doi.org/10.2351/1.3267476

Schaefer, M., Kessler, S., Fetzer, F., & Graf, T. (2017). Influence of the focal position on the melt flow during laser welding of steel. *Journal of Laser Applications*, *29*(1), 012010. https://doi.org/10.2351/1.4972098

Sokolov, M., Franciosa, P., Al Botros, R., & Ceglarek, D. (2020). Keyhole mapping to enable closed-loop weld penetration depth control for remote laser welding of aluminum components using optical coherence tomography. *Journal of Laser Applications*, *32*(3), 032004. https://doi.org/10.2351/7.0000086

Sokolov, M., Franciosa, P., Sun, T., Ceglarek, D., Dimatteo, V., Ascari, A., et al. (2020). Applying optical coherence tomography for weld depth monitoring in remote laser welding of automotive battery tab connectors. *Journal of Laser Applications*, *33*(1), 012028. https://doi.org/10.2351/7.0000336

Um, J., & Stroud, I. A. (2017). Design guidelines for remote laser welding in automotive assembly lines. *The International Journal of Advanced Manufacturing Technology*, *89*(1–4), 1039–1051. https://doi.org/10.1007/s00170-016-9096-0

Wang, R., Lei, Y., & Shi, Y. (2011). Numerical simulation of transient temperature field during laser keyhole welding of 304 stainless steel sheet. *Optics & Laser Technology*, *43*(4), 870–873. https://doi.org/10.1016/j.optlastec.2010.10.007

You, D., Gao, X., & Katayama, S. (2013). Multiple-optics sensing of high-brightness disk laser welding process. *NDT & E International*, *60*, 32–39. https://doi.org/10.1016/j.ndteint.2013.07.005